ARTICLE

Improved Synthesis of Graphene Oxide

Daniela C. Marcano,[†] Dmitry V. Kosynkin,[†] Jacob M. Berlin, Alexander Sinitskii, Zhengzong Sun, Alexander Slesarev, Lawrence B. Alemany, Wei Lu, and James M. Tour*

Departments of Chemistry, Mechanical Engineering and Materials Science, and the Smalley Institute for Nanoscale Science and Technology, Rice University, MS 222, 6100 Main Street, Houston, Texas 77005. [†]These authors contributed equally to this work.

ABSTRACT An improved method for the preparation of graphene oxide (GO) is described. Currently, Hummers' method ($KMnO_4$, $NaNO_3$, H_2SO_4) is the most common method used for preparing graphene oxide. We have found that excluding the $NaNO_3$, increasing the amount of $KMnO_4$, and performing the reaction in a 9:1 mixture of H_2SO_4/H_3PO_4 improves the efficiency of the oxidation process. This improved method provides a greater amount of hydrophilic oxidized graphene material as compared to Hummers' method or Hummers' method with additional $KMnO_4$. Moreover, even though the GO produced by our method is more oxidized than that prepared by Hummers' method, when both are reduced in the same chamber with hydrazine, chemically converted graphene (CCG) produced from this new method is equivalent in its electrical conductivity. In contrast to Hummers' method, the new method does not generate toxic gas and the temperature is easily controlled. This improved synthesis of GO may be important for large-scale production of GO as well as the construction of devices composed of the subsequent CCG.

KEYWORDS: graphene · graphite · oxide · carbon · nanostructure

Graphene has enjoyed significant recent attention.[1] Graphene is a single atomic layer of sp^2 carbon atoms. Few- and single-layer transferable graphene nanosheets were first obtained by mechanical exfoliation ("Scotch-tape" method) of bulk graphite[2] and by epitaxial chemical vapor deposition.[3] Although those routes might be preferred for precise device assembly, they can be less effective for large-scale manufacturing. Chemical means are a practical approach to bulk-scale graphene materials.[4] The primary obstacle to achieving individual or few-layer graphene is overcoming the enormous interlayer van der Waals forces. To date, chemical efforts at graphite exfoliation have been focused primarily on intercalation, chemical derivatization, thermal expansion, oxidation−reduction, the use of surfactants, or some combination thereof.[5−13]

The most common approach to graphite exfoliation is the use of strong oxidizing agents to yield graphene oxide (GO), a nonconductive hydrophilic carbon material.[14−17]Although the exact structure of GO is difficult to determine, it is clear that for GO the previously contiguous aromatic lattice of graphene is interrupted by epoxides, alcohols, ketone carbonyls, and carboxylic groups.[18−20] The disruption of the lattice is reflected in an increase in interlayer spacing from 0.335 nm for graphite to more than 0.625 nm for GO.[21] Brodie first demonstrated the synthesis of GO in 1859 by adding a portion of potassium chlorate to a slurry of graphite in fuming nitric acid.[22] In 1898, Staudenmaier improved on this protocol by using concentrated sulfuric acid as well as fuming nitric acid and adding the chlorate in multiple aliquots over the course of the reaction. This small change in the procedure made the production of highly oxidized GO in a single reaction vessel significantly more practical.[23] In 1958, Hummers reported the method most commonly used today: the graphite is oxidized by treatment with $KMnO_4$ and $NaNO_3$ in concentrated H_2SO_4.[15] It should be noted that all three of these procedures involve the generation of the toxic gas(es) NO_2, N_2O_4, and/or ClO_2; the latter also being explosive.

The most common source of graphite used for chemical reactions, including its oxidation, is flake graphite, which is a naturally occurring mineral that is purified to remove heteroatomic contamination.[24] GO prepared from flake graphite can be readily dispersed in water and has been used on a large scale for preparing large graphitic films, as a binder for carbon products, and as a component of the cathode of lithium batteries.[25−28] Moreover, the hydrophilicity of GO allows it to be uniformly deposited onto substrates in the form of thin films, which is necessary for applications in electronics.[29] It is also often essential that the GO can be transformed back into a conduc-

*Address correspondence to tour@rice.edu.

Received for review March 29, 2010 and accepted July 12, 2010.

Published online July 22, 2010.
10.1021/nn1006368

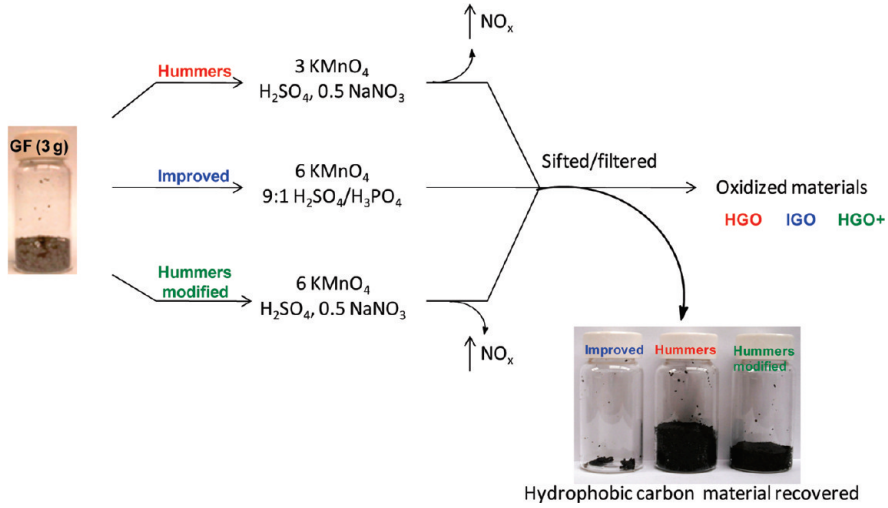

Figure 1. Representation of the procedures followed starting with graphite flakes (GF). Under-oxidized hydrophobic carbon material recovered during the purification of IGO, HGO, and HGO+. The increased efficiency of the IGO method is indicated by the very small amount of under-oxidized material produced.

tive graphitic material, and indeed, either in thin films or in bulk, partial restoration of the graphitic structure can be accomplished by chemical reduction[12,29−31] to chemically converted graphene (CCG). However, the graphitic structure (with its desired properties) is not fully restored using these conditions, and significant defects are introduced.[32]

Recently, we reported the scalable preparation of graphene oxide nanoribbons (GONRs) from multiwalled carbon nanotubes by treatment with $KMnO_4$ and concentrated H_2SO_4[30] and the discovery that the addition of phosphoric acid (H_3PO_4) to this reaction produced GONRs with more intact graphitic basal planes.[33] Reduction of these second-generation GONRs produced ribbons that were comparable in conductivity to those prepared by reduction of the first-generation GONRs. We hypothesized that this oxidation procedure ($KMnO_4$ and a 9:1 mixture of concentrated H_2SO_4/H_3PO_4, called the "improved method" for clarity of discussion in this paper) could be used to prepare improved GO (IGO) with fewer defects in the basal plane as compared to GO prepared by the Hummers' method. The IGO synthesis was evaluated in comparison to Hummers' method or Hummers' method with additional $KMnO_4$. For clarity, we have named the GO produced by these methods: IGO, HGO, and HGO+, respectively. The improved method provides a greater amount of hydrophilic oxidized graphite material relative to the other two procedures. Moreover, even though IGO is as oxidized as HGO+ and both are more oxidized than HGO, IGO has a more regular structure with a greater amount of basal plane framework retained. This is reflected in the fact that, when all three GOs are reduced with hydrazine hydrate, the CCG produced from IGO (CCIG) showed an equivalent level of conductivity with respect to the material produced from the other two methods (CCHG, CCHG+). The advantages of the improved method, with its simpler protocol, higher yield, no toxic gas evolution during preparation, and equivalent conductivity upon reduction, make it attractive for preparing material on a large scale. It may also show improved performance in materials applications, such as in membranes, TEM grids, or temperature-sensitive device fabrication.

DISCUSSION

The increased efficiency of the IGO method as compared to the HGO and HGO+ methods was apparent after the first purification step for each method. The hydrophilic carbon material produced during the reaction passed through the sieve, while the under-oxidized hydrophobic carbon material was retained on the sieve due to its particle size and low water solubility. Significantly less under-oxidized material was generated in the production of IGO (0.7 g) compared to HGO (6.7 g) or HGO+ (3.9 g) when starting with 3 g of graphite flakes. Note that these weights correspond to the under-oxidized graphene and any water that was retained after drying overnight in vacuum; the HGO and HGO+ had a wet appearance (Figure 1).

Following purification, the hydrophilic materials obtained (IGO, HGO, HGO+) were characterized. Raman and infrared spectroscopy indicated that all three materials were grossly similar. Raman spectra show D peaks ~1590 cm^{-1} and G peaks ~1350 cm^{-1}, confirming the lattice distortions (Figure 2A). Also, FTIR-ATR spectra (Figure 2B) were recorded, and the following functional groups were identified in all samples: O−H stretching vibrations (3420 cm^{-1}), C═O stretching vibration (1720−1740 cm^{-1}), C═C from unoxidized sp^2 CC bonds (1590−1620 cm^{-1}), and C−O vibrations (1250 cm^{-1}).

Atomic force microscopy (AFM) images (Figure 3) also indicated that the three materials were grossly similar, as the thicknesses of the IGO, HGO+, and HGO layers were all ~1.1 nm.

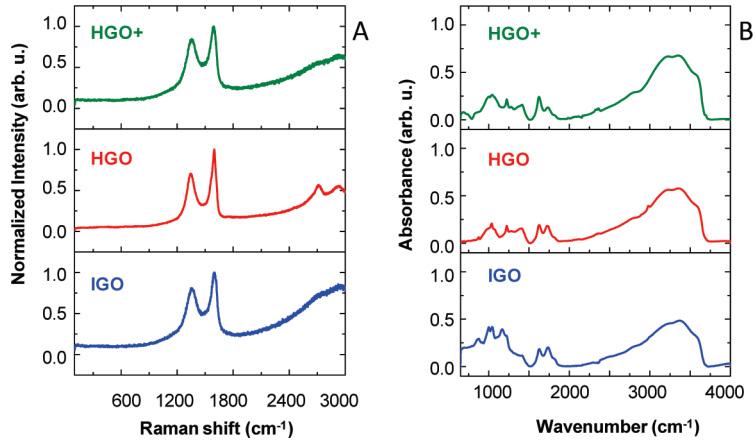

Figure 2. (A) Raman spectra recorded using 514 nm laser excitation and (B) FTIR-ATR spectra of HGO+, HGO, and IGO.

A variety of techniques indicated that the order of overall oxidation is HGO < HGO+ < IGO. Thermogravimetric analysis (TGA) of the materials (Figure 4) showed major weight losses between 150 and 300 °C, which corresponds to CO, CO_2, and steam release[10] from the most labile functional groups. Between 400 and 950 °C, a slower mass loss was observed and can be attributed to the removal of more stable oxygen functionalities.[34] By TGA, HGO had the smallest weight loss while HGO+ and IGO had similar weight losses.

Solid-state ^{13}C NMR (Figure 5) suggests that the order of overall oxidation is HGO < HGO+ < IGO. The sig-

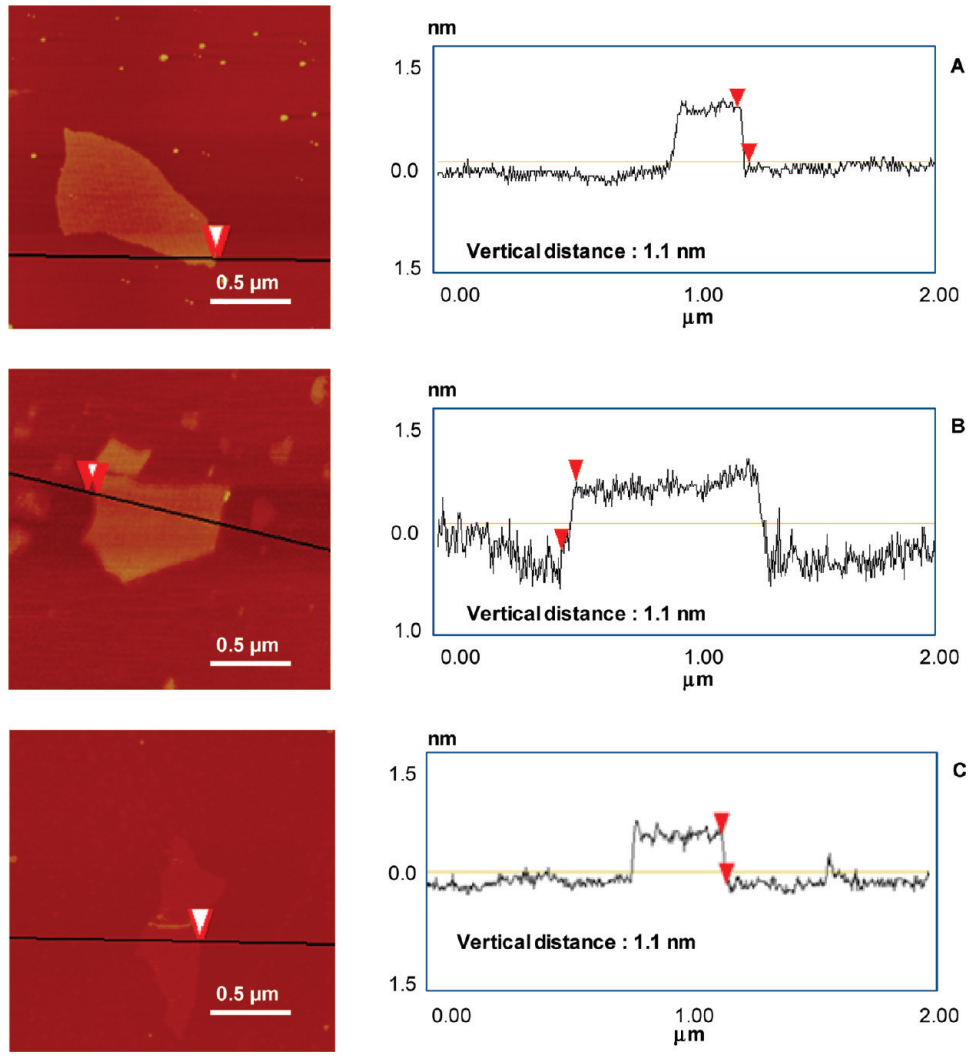

Figure 3. Tapping mode AFM topographic images and height profiles of a single layer of (A) HGO+, (B) HGO, and (C) IGO.

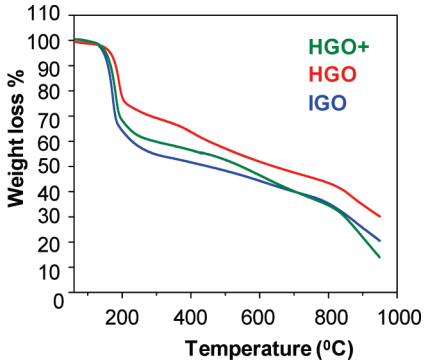

Figure 4. TGA plots of HGO+, HGO, and IGO.

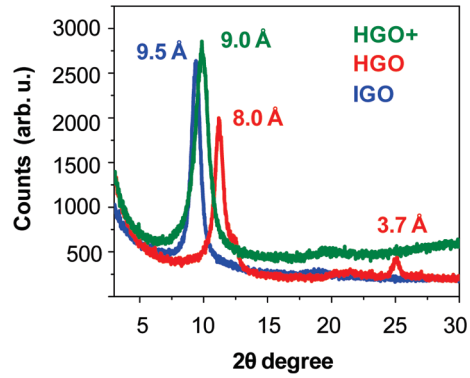

Figure 6. XRD spectra of HGO, HGO+, and IGO (1.54059 Å Cu Kα 1 as wavelength).

nals can be assigned as described previously:[10,35,36] ketone carbonyls near 190 ppm; ester and lactol carbonyls near 164 ppm; graphitic sp^2 carbons near 131 ppm; lactols O−C(sp^3)−O near 101 ppm; and alcohols at about 70 ppm with an upfield intense signal from epoxides near 61 ppm. The simplest measure of oxidation is the ratio between the alcohol/epoxide signal and graphitic sp^2 carbon signal. This ratio is greatest for IGO and least for HGO. It is also noteworthy that IGO appears to have more epoxide functionalities than either of the other GOs.

The X-ray diffraction (XRD) spectra (Figure 6) support the same order of overall oxidation. For XRD, the interlayer spacing of the materials is proportional to the degree of oxidation. The spacings are 9.5, 9.0, and 8.0 Å for IGO, HGO+, and HGO, respectively. Also, the HGO spectrum had a peak at 3.7 Å, indicating that traces of starting material (graphite flakes) were present in the sample.

The X-ray photoelectron spectroscopy (XPS) spectra of the samples both support the conclusion that IGO is the most oxidized material and suggest that the IGO has a more organized structure than the other two materials. To determine the relative levels of oxidation, the C/O ratio was not used; it is unreliable because it is difficult to fully dehydrate a GO sample.[37] Instead, the C1s spectra were compared by deconvoluting (Multipack software, version 7.0) each spectrum into four peaks that correspond to the following functional groups: carbon sp^2 (C═C, 284.8 eV), epoxy/hydroxyls (C−O, 286.2 eV), carbonyl (C═O, 287.8 eV), and carboxylates (O−C═O, 289.0 eV).[10] All percentages of the oxidized materials were combined such that IGO had 69% oxidized carbon and 31% graphitic carbon; HGO+ had 63 and 37%; HGO contained 61 and 39% of the oxidized carbon and graphitic carbon, respectively. The C1s XPS spectra were then normalized with respect to the C═C peak (Figure 7). The degree of oxidation for each sample is similar to the amount indicated by ^{13}C NMR. IGO is the most oxidized material, HGO+ is slightly (~10%) less oxidized, and HGO is the least oxidized. Moreover, the apparent peak at ~287 eV, corresponding to the oxidized carbons for IGO, is sharper than the same peak for HGO+. This suggests that, for similar levels of overall oxidation, the IGO has a more regular structure than that of HGO+.[38]

Transmission electron microscopy (TEM) images of the three samples support the assertion that IGO has a more regular structure than either HGO+ or HGO (Figure 8). All three procedures produce large flakes of GO that are a few layers thick; however, the diffraction patterns indicate differences in crystallinity. HGO is modestly crystalline, but when the more highly oxidized HGO+ is analyzed, an amorphous structure is indicated by the diffuse diffraction pattern.[29,39] In comparison, the IGO is highly oxidized but has the sharpest diffraction pattern of all three samples, again suggesting that IGO has a more regular carbon framework than HGO or HGO+.

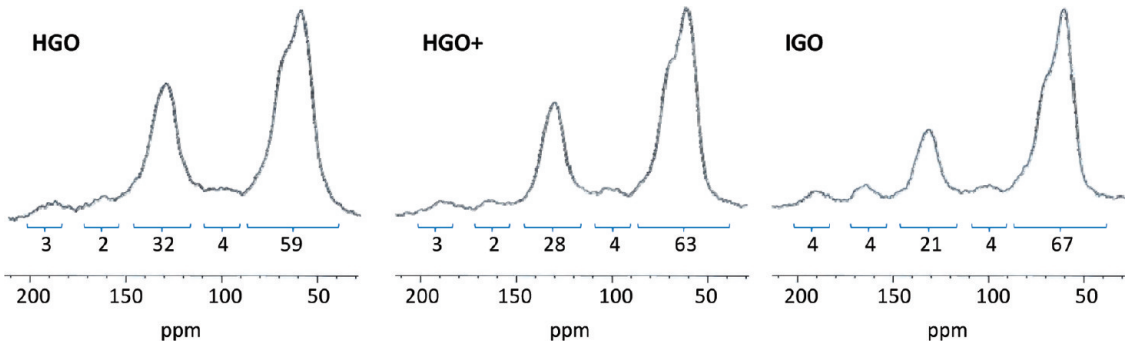

Figure 5. ^{13}C NMR (50.3 MHz) spectra obtained of HGO, HGO+ and IGO [12 kHz magic angle spinning (MAS), a 90° ^{13}C pulse, 41 ms FID, and 20 s relaxation delay]. Integration areas are shown under each peak.

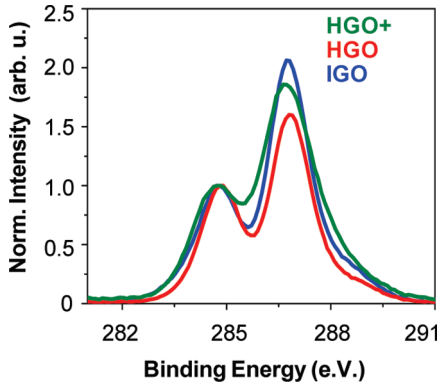

Figure 7. C1s XPS spectra of HGO+, HGO, and IGO normalized with respect to the C═C peak.

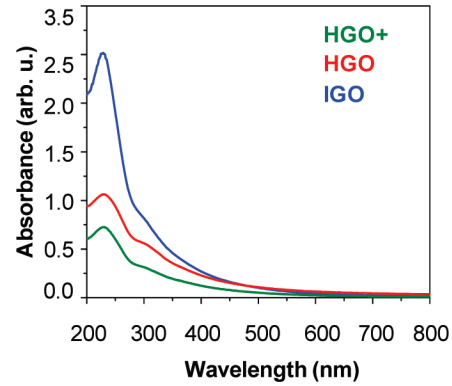

Figure 9. UV/vis spectra recorded in aqueous solutions at 0.05 mg/mL of HGO+, HGO, and IGO.

The UV/vis spectra of the three materials suggest that the more ordered structure of IGO is due to greater retention of carbon rings in the basal planes. The three spectra were recorded for an equal concentration of each material (Figure 9). The degree of remaining conjugation can be determined by the λ_{max} of each UV/vis spectrum. The more $\pi \rightarrow \pi^*$ transitions (conjugation), the less energy needs to be used for the electronic transition, which results in a higher λ_{max}. IGO, HGO+, and HGO all have a very similar λ_{max}, which is in the 227−231 nm range as previously reported for GO.[12,40] Also, for all three materials, a similar shoulder around ~300 nm is observed and can be attributed to $n \rightarrow \pi^*$ transitions of the carbonyl groups. This suggests that the materials are grossly similar in structure, as the Raman, IR, and AFM data indicated. However, IGO has a larger extinction coefficient than those of HGO+ or HGO, suggesting that, for an equal amount of each sample, the IGO has more aromatic rings or isolated aromatic domains retained. The λ_{max} data indicate that these aromatic rings are not in extended conjugation, but the overall absorption indicates that IGO has more aromatic rings retained.

Bulk samples of the oxidized materials were reduced using hydrazine hydrate and then annealed at 300 and 900 °C in Ar/H_2. In general, for the hydrazine reduction, 100 mg of the IGO, HGO, or HGO+ material was dispersed in 100 mL of DI water, stirred for 30 min, and then 1.00 mL of hydrazine hydrate was added. The mixtures were heated at 95 °C using a water bath for 45 min; a black solid precipitated from the reaction mixture. Products were isolated by filtration (PTFE 20 μm pore size) and washed with DI water (50 mL, 3×) and methanol (20 mL, 3 ×), producing 54, 57, and 76 mg of the reduced chemically converted IGO (CCIG), chemically converted HGO+ (CCHG+), and chemically converted HGO (CCHG), respectively. After reduction, no signal from oxidized carbons could be detected by NMR. Only a broad aromatic/alkene NMR signal could be detected for CCHG, CCHG+, and CCIG. This signal was shifted upfield relative to that in the precursor HGO, HGO+, and IGO; the peak maximum after reduction was at about 118 ppm, very similar to that noted previously[35] on other samples of reduced GO. Reduction also had an effect similar to that previously noted[35] on the drive pressure required to spin the rotor and on

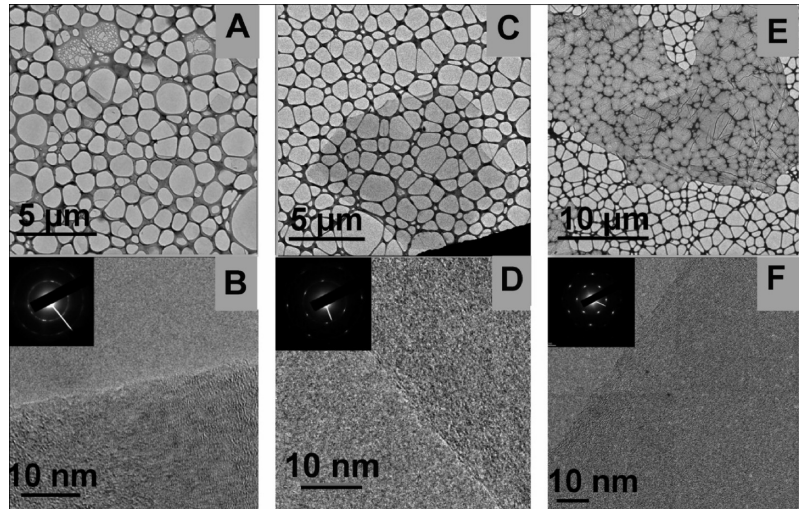

Figure 8. TEM images of (A) HGO+, (C) HGO, (E) IGO and their diffraction patterns (B), (D), and (F), respectively. Insets are the selected area electron diffraction (SAED) patterns corresponded to the graphene films in the TEM images. TEM grids with lacey carbon support films (Ted Pella, Inc.) were used to prepare the samples.

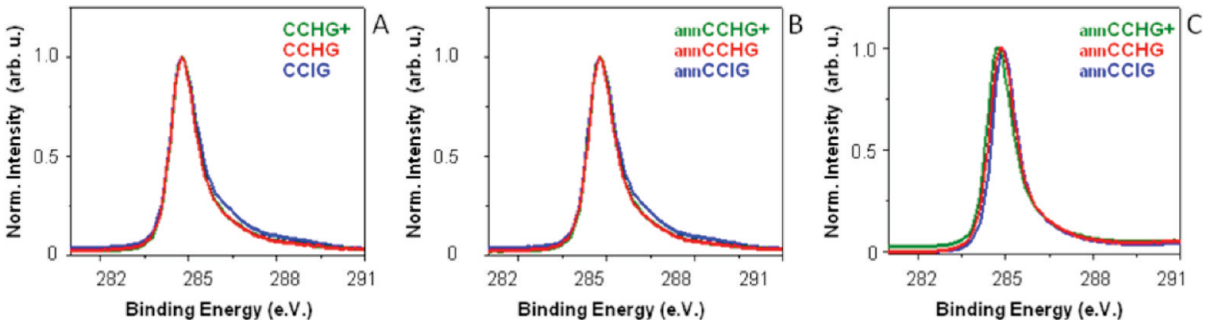

Figure 10. C1s XPS spectra of (A) hydrazine reduced, (B) further 300 °C/H_2-annealed materials, (C) 900 °C/H_2-annealed materials. The annealed materials in panels B and C are designated by the prefix "ann" to differentiate them from the materials in A that were only hydrazine reduced.

the tuning and matching of the ^{13}C and ^{1}H channels of the probe. After reduction and annealing in Ar/H_2 at 900 °C, no NMR signal could be detected for any of the samples, consistent with their becoming even more graphite-like.[35]

XPS analysis of the black solids showed similar levels of reduction for all three materials when they were hydrazine reduced and when they were annealed (Figure 10; in Figure 10B,C, the annealed materials are designated by the prefix "ann" to differentiate them from the materials that were only hydrazine reduced). Atomic compositions were C(1s) 89%, N(1s) 3%, and O(1s) 8% for CCHG+; C(1s) 88%, N(1s) 3%, and O(1s) 9% for CCHG; and C(1s) 86%, N(1s) 5%, O(1s) 9%, and P(2p) <0.1% for CCIG (the amount is lower than the detection level of the instrument).

In order to estimate the degree of graphitization with greater precision for each material after being reduced, electrical conductivities were measured. Figure 11A,B displays scanning electron microscopy (SEM) images of typical CCIG flakes, which were deposited on a Si/SiO_2 substrate and then reduced by hydrazine vapor. For the hydrazine vapor reduction, Si/SiO_2 substrates coated with GO were deposited inside a beaker with 0.5 mL of hydrazine hydrate and covered with foil. The system was heated using a water bath at 95 °C for 45 min. The material was well-exfoliated; the majority of the flakes on the chip were only a few layers thick and several tens of micrometers in diameter. As an example, Figure 11A shows an individual flake, which is 60 μm in diameter and, based on AFM data, is only 2 nm thick. Typically, the thicknesses of monolayer GO flakes are in the range of 0.7−1 nm,[10,40−43] so the shown flake most likely consists of two layers. The largest flake in Figure 11B is 160 μm in diameter.

As-prepared HGO, HGO+, and IGO flakes were deposited on Si/SiO_2 substrates (heavily doped p-type Si with a 500 nm thermal SiO_2 layer), dried in air, and then reduced by hydrazine vapor in the same flask so that they were exposed to identical reaction conditions. Individual flakes of reduced graphene materials with thicknesses ranging from 1 to 3 nm were selected for device fabrication. Electronic devices were patterned by standard e-beam lithography (we used PMMA as a positive resist), and then 20 nm thick Pt contacts were formed by e-beam evaporation and lift-off process. Figure 11C shows a SEM image of a typical electronic device.

The electrical measurements were performed using a probe station (Desert Cryogenics TT-probe 6 system) under vacuum with chamber base pressure below 10^{-5} Torr. Normally, the devices were kept under vacuum for at least 2 days before the measurements. The current−voltage (*IV*) data were collected on an Agilent 4155C semiconductor parameter analyzer. All CCG flakes in the fabricated electronic devices exhibited qualitatively the same electrical properties. They behaved as p-type semiconductors in air but exhibited ambipolar electric field effect in vacuum after several days of evacuation in the probe station chamber at $\sim 10^{-5}$ Torr (Figure 11D).[31,44−46] This effect can be attributed to the desorption of the atmospheric adsorbates that are known to cause doping effects in graphene.[47] This effect was completely reversible; after exposure to air, the CCG flakes again behaved as p-type semiconductors. For the monolayer (with thickness of about 1 nm) CCHG, CCHG+, and CCIG flakes, we also compared electrical properties. CCHG and CCHG+ devices exhibited approximately the same conductivity values of ~0.05 S/cm, whereas CCIG monolayers were about twice as conductive (~0.1 S/cm); the above numbers were averaged for 3−5 devices. However, considering significant variability in conductivities, found by us for each set of the devices and also reported elsewhere,[42] it is difficult to conclude whether or not hydrazine reduced IGO flakes are indeed more conductive than their HGO and HGO+ counterparts. Importantly, these numbers where obtained by four-probe technique for the flakes that were hydrazine reduced from the original materials under the same conditions.

Since the hydrazine reduction was not sufficient to achieve high conductivities of the flakes, we further reduced the CCG materials by annealing in Ar/H_2 at high temperatures. Additionally, we fabricated electronic devices based on monolayer CCHG, CCHG+, and CCIG

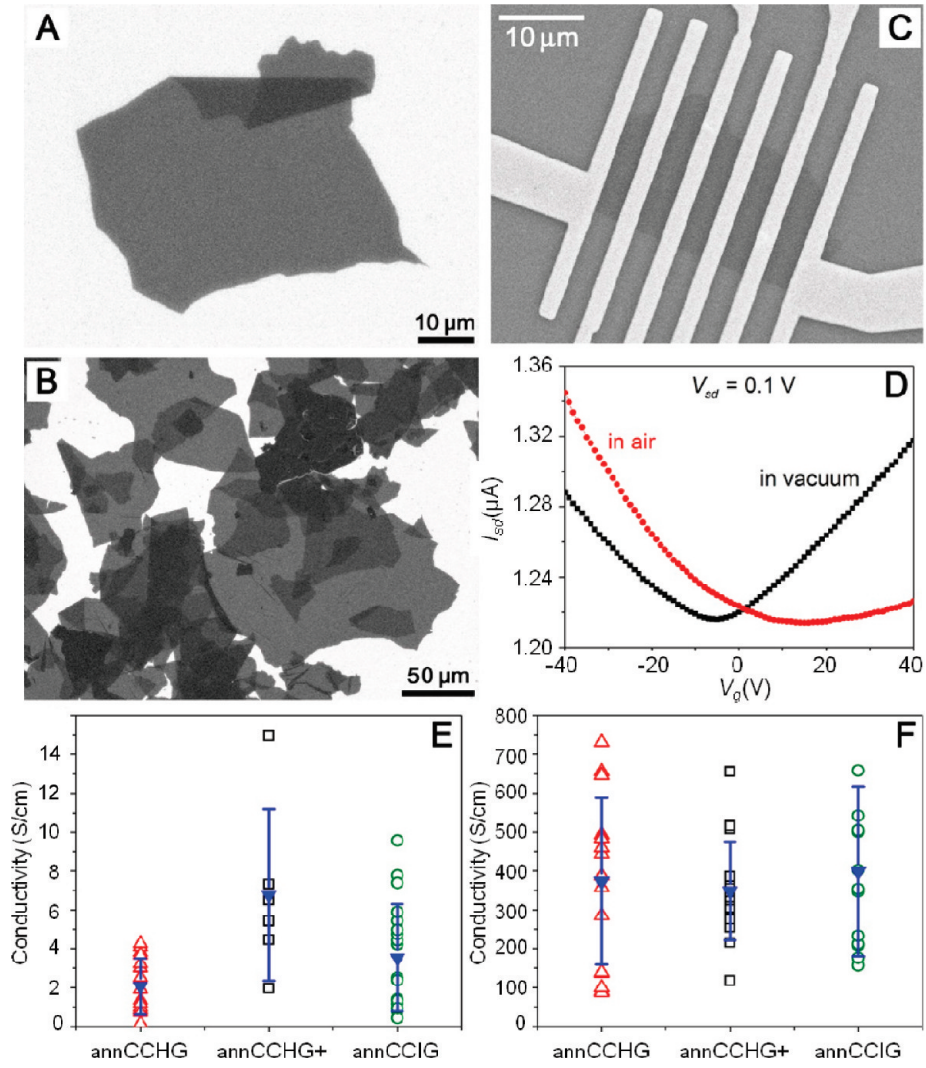

Figure 11. (A,B) SEM images of CCIG flakes on Si/SiO_2 substrate. (C) SEM image of a typical electronic device for a hydrazine reduced CCIG flake. (D) Source−drain current (I_{sd})−gate voltage (V_g) characteristics of the same electronic device based on a few-layer CCIG flake measured in air and in vacuum after 3 days of evacuation in the probe station chamber at the pressure of $\sim 10^{-5}$ Torr. (E) Plot of the mean conductivities for the monolayer annCCHG, annCCHG+, and annCCIG flakes annealed in Ar/H_2 at 300 °C for 0.5 h. (F) Plot of the mean conductivities for the monolayer annCCHG, annCCHG+, and annCCIG flakes annealed in Ar/H_2 at 900 °C for 0.5 h.

flakes annealed in Ar/H_2 at 300 or 900 °C for 0.5 h. For these thermally annealed materials, we measured at least six devices for each material. We found that, after the thermal treatment at 300 °C, the conductivities of the annCCG materials dramatically increase up to 2.1 ± 1.4 S/cm (annCCHG), 6.8 ± 4.4 S/cm (annCCHG+), and 3.5 ± 2.5 S/cm (annCCIG); the scatter plot is shown in Figure 11E. The annCCHG is statistically significantly less conductive than the other two samples ($p < 0.05$, t test assuming equal variance), but due to the small number of devices for annCCHG+, it is difficult to determine if the annCCHG+ and annCCIG are significantly different. The statistical significance of the increase in conductivity for annCCHG+ compared to annCCIG is marginal ($p = 0.04$, t test assuming equal variance) and completely driven by the outlier point at 15.0 (removing this point, $p = 0.24$, t test assuming equal variance). Here, as well as in other cases, the conductivities were calculated assuming the thicknesses of the flakes to be 1 nm. CCG materials annealed at even higher temperature of 900 °C exhibit further increases in conductivities up to 375 ± 215 S/cm (annCCHG), 350 ± 125 S/cm (annCCHG+), and 400 ± 220 S/cm (annCCIG) (Figure 11F). There is no statistically significant difference between any of the samples after annealing at 900 °C, suggesting that high temperature annealing eliminates most of the differences in composition and structure present in the three samples.

CONCLUSIONS

The improved method for producing GO has significant advantages over Hummers' method. The protocol for running the reaction does not involve a large exotherm and produces no toxic gas. Moreover, the improved method yields a higher fraction of well-oxidized hydrophilic carbon material. This IGO is more oxidized

than HGO and slightly more oxidized than HGO+. The IGO possesses a more regular structure than the other materials. An increased number of isolated aromatic rings could be a component of this more regular framework structure. This suggests that the improved method might disrupt the basal plane of the graphite less than Hummers' method. The mechanism for producing IGO with a more regular structure could be based on the formation of five-membered cyclic phosphate groups between the phosphoric acid and two vicinal diols formed on the graphite basal plane.[33] Taken together, these data suggest that the improved method could be advantageous for large-scale production of GO.

EXPERIMENTAL PROCEDURES

Graphite flakes (Sigma-Aldrich, cat #332461, ~150 μm flakes) were oxidized using three different procedures: improved method, Hummers' method, and Hummers' method with additional $KMnO_4$.

For the improved method, a 9:1 mixture of concentrated H_2SO_4/H_3PO_4 (360:40 mL) was added to a mixture of graphite flakes (3.0 g, 1 wt equiv) and $KMnO_4$ (18.0 g, 6 wt equiv), producing a slight exotherm to 35−40 °C. The reaction was then heated to 50 °C and stirred for 12 h. The reaction was cooled to rt and poured onto ice (~400 mL) with 30% H_2O_2 (3 mL). For workup, the mixture was sifted through a metal U.S. Standard testing sieve (W.S. Tyler, 300 μm) and then filtered through polyester fiber (Carpenter Co.) The filtrate was centrifuged (4000 rpm for 4 h), and the supernatant was decanted away. The remaining solid material was then washed in succession with 200 mL of water, 200 mL of 30% HCl, and 200 mL of ethanol (2×); for each wash, the mixture was sifted through the U.S. Standard testing sieve and then filtered through polyester fiber with the filtrate being centrifuged (4000 rpm for 4 h) and the supernatant decanted away. The material remaining after this extended, multiple-wash process was coagulated with 200 mL of ether, and the resulting suspension was filtered over a PTFE membrane with a 0.45 μm pore size. The solid obtained on the filter was vacuum-dried overnight at room temperature, obtaining 5.8 g of product.

For Hummers' method, concentrated H_2SO_4 (69 mL) was added to a mixture of graphite flakes (3.0 g, 1 wt equiv) and $NaNO_3$ (1.5 g, 0.5 wt equiv), and the mixture was cooled to 0 °C. $KMnO_4$ (9.0 g, 3 wt equiv) was added slowly in portions to keep the reaction temperature below 20 °C. The reaction was warmed to 35 °C and stirred for 30 min, at which time water (138 mL) was added slowly, producing a large exotherm to 98 °C. External heating was introduced to maintain the reaction temperature at 98 °C for 15 min, then the heat was removed and the reaction was cooled using a water bath for 10 min. Additional water (420 mL) and 30% H_2O_2 (3 mL) were added, producing another exotherm. After air cooling, the mixture was purified as described for the IGO above (sifting, filtration, multiple washings, centrifugations and decanting, vacuum drying) to give 1.2 g of solid.

The third method makes use of the Hummers' reagents with additional $KMnO_4$. We call this method Hummers' method+ and its product HGO+. Concentrated H_2SO_4 (69 mL) was added to a mixture of graphite flakes (3.0 g, 1 wt equiv) and $NaNO_3$ (1.5 g, 0.5 wt equiv), and the mixture was cooled using an ice bath to 0 °C. $KMnO_4$ (9.0 g, 3 wt equiv) was added slowly in portions to keep the reaction temperature below 20 °C. The reaction was warmed to 35 °C and stirred for 7 h. Additional $KMnO_4$ (9.0 g, 3 wt equiv) was added in one portion, and the reaction was stirred for 12 h at 35 °C. The reaction mixture was cooled to room temperature and poured onto ice (~400 mL) with 30% H_2O_2 (3 mL). The mixture was then purified following the previous protocol of sifting, filtering, centrifugation, decanting with multiple washes followed by a final vacuum drying to give 4.2 g of solid product.

Acknowledgment. We thank the Alliance for Nanohealth (W8XWH-07-2-0101), M-I-SWACO, Air Force Research Laboratory through University Technology Corporation, 09-S568-064-01-C1, U.S. Department of Energy's Office of Energy Efficiency and Renewable Energy within the Hydrogen Sorption Center of Excellence, DE-FC-36-05GO15073, the Office of Naval Research MURI program on graphene, the AFOSR, FA9550-09-1-0581, and the Federal Aviation Administration (2007G010) for financial support.

REFERENCES AND NOTES

1. Geim, A. K.; Novoselov, K. S. The Rise of Graphene. *Nat. Mater.* **2007**, *6*, 183–191.
2. Novoselov, K. S.; Geim, A. K.; Morozov, S. V.; Jiang, D.; Zhang, Y.; Dubonos, S. V.; Grigorieva, I. V.; Firsov, A. A. Electric Field Effect in Atomically Thin Carbon Films. *Science* **2004**, *306*, 666–669.
3. Berger, C.; Song, Z.; Li, X.; Wu, X.; Brown, N.; Naud, C.; Mayou, D.; Li, T.; Hass, J.; Marchenkov, A. N.; Conrad, E. H.; First, P. N.; de Heer, W. A. Electronic Confinement and Coherence in Patterned Epitaxial Graphene. *Science* **2006**, *312*, 1191–1196.
4. Ruoff, R. Graphene Calling All Chemists. *Nat. Nanotechnol.* **2008**, *3*, 10–11.
5. Chakraborty, S.; Guo, W.; Hauge, R. H.; Billups, W. E. Reductive Alkylation of Fluorinated Graphite. *Chem. Mater.* **2008**, *20*, 3134–3136.
6. Schniepp, H. C.; Li, J. L.; McAllister, M. J.; Sai, H.; Herrera-Alonso, M.; Adamson, D. H.; Prud'homme, R. K.; Car, R.; Saville, D. A.; Aksay, I. A. Functionalized Single Graphene Sheets Derived from Splitting Graphite Oxide. *J. Phys. Chem. B* **2006**, *110*, 8535–8539.
7. Si, Y.; Samulski, E. T. Synthesis of Water Soluble Graphene. *Nano Lett.* **2008**, *8*, 1679–1682.
8. Lomeda, J. R.; Doyle, C. D.; Kosynkin, D. V.; Hwang, W. F.; Tour, J. M. Diazonium Functionalization of Surfactant-Wrapped Chemically Converted Graphene Sheets. *J. Am. Chem. Soc.* **2008**, *130*, 16201–16206.
9. Behabtu, N.; Lomeda, J. R.; Green, M. J.; Higginbotham, A. L.; Sinitskii, A.; Kosynkin, D. V.; Tsentalovich, D.; Parra-Vasquez, A. N. G.; A; Schmidt, J.; Kesselman, E.; Cohen, Y.; Talmon, Y.; Tour, J. M.; Pasquali, M. Spontaneous High-Concentration Dispersions and Liquid Crystals of Graphene. *Nat. Nanotechnol.* **2010**, *5*, 406–411.
10. Stankovich, S.; Dikin, D. A.; Piner, R. D.; Kohlhaas, K. A.; Kleinhammes, A.; Jia, Y.; Wu, Y.; Nguyen, S. B. T.; Ruoff, R. S. Synthesis of Graphene-Based Nanosheets via Chemical Reduction of Exfoliated Graphite Oxide. *Carbon* **2007**, *45*, 1558–1565.
11. Xu, Y.; Bai, H.; Lu, G.; Li, C.; Shi, G. Flexible Graphene Films *via* the Filtration of Water-Soluble Noncovalent Functionalized Graphene Sheets. *J. Am. Chem. Soc.* **2008**, *130*, 5856–5857.
12. Li, D.; Mueller, M. B.; Gilje, S.; Kaner, R. B.; Wallace, G. G. Processable Aqueous Dispersions of Graphene Nanosheets. *Nat. Nanotechnol.* **2008**, *3*, 101–105.
13. Lotya, M.; Hernandez, Y.; King, P. J.; Smith, R. J.; Nicolosi, V.; Karlsson, L. S.; Blighe, F. M.; De, S.; Wang, Z.; McGovern, I. T.; Duesberg, G. S.; Coleman, J. N. Liquid Phase Production of Graphene by Exfoliation of Graphite in Surfactant/Water Solutions. *J. Am. Chem. Soc.* **2009**, *131*, 3611–3620.

14. Higginbotham, A. L.; Lomeda, J. R.; Morgan, A. B.; Tour, J. M. Graphite Oxide Flame-Retardant Polymer Nanocomposites. *Appl. Mater. Interfaces* **2009**, *1*, 2256–2261.
15. Hummers, W. S.; Offeman, R. E. Preparation of Graphitic Oxide. *J. Am. Chem. Soc.* **1958**, *80*, 1339.
16. Lerf, A.; He, H.; Forster, M.; Klinowski, J. Structure of Graphite Oxide Revisited. *J. Phys. Chem. B* **1998**, *102*, 4477–4482.
17. Dreyer, D. R.; Park, S.; Bielawski, C. W.; Ruoff, R. The Chemistry of Graphene Oxide. *Chem. Soc. Rev.* **2010**, *39*, 228–240.
18. He, H.; Klinowski, J.; Forster, M. A New Structural Model for Graphite Oxide. *Chem. Phys. Lett.* **1998**, *287*, 53–56.
19. Uhl, F.; Wilkie, C. Preparation of Nanocomposites from Styrene and Modified Graphite Oxides. *Polym. Degrad. Stab.* **2004**, *84*, 215–226.
20. Stankovich, S.; Piner, R.; Chen, X.; Wu, N.; Nguyen, S.; Ruoff, R. Stable Aqueous Dispersions of Graphitic Nanoplatelets *via* the Reduction of Exfoliated Graphite Oxide in the Presence of Poly(sodium 4-styrenesulfonate). *J. Mater. Chem* **2006**, *16*, 155–158.
21. Hontoria- Lucas, C.; López-Peinado, A.; López-González, J.; Rojas-Cervantes, M.; Martín-Aranda, R. Study of Oxygen-Containing Groups in a Series of Graphite Oxides: Physical and Chemical Characterization. *Carbon* **1995**, *33*, 1585–1592.
22. Brodie, B. C. On the Atomic Weight of Graphite. *Philos. Trans. R. Soc. London* **1859**, *14*, 249–259.
23. Staudenmaier, L. Verfahren zur Darstellung der Graphitsäure. *Ber. Dtsch. Chem. Ges.* **1898**, *31*, 1481–1487.
24. Wissler, M. Graphite and Carbon Powders for Electrochemical Applications. *J. Power Sources* **2006**, *156*, 142–150.
25. Ishikawa, T.; Nagaoki, T. *Shin tanso kogyo (New Carbon Industry)*, 2nd ed.; Kindai hensyusya: Tokyo, 1986; pp 125–36.
26. Maire, J.; Colas, H.; Maillard, P. Membranes de Carbone et de Graphite et Leurs Proprieties. *Carbon* **1968**, *6*, 555–560.
27. Ishikawa, T.; Kanemaru, T.; Teranishi, H.; Onishi, K. Composites of Oxidized Graphite Material and Expanded Graphite Material. U.S. Patent 4094951, June 13, 1978.
28. Touzain, P.; Yazumi, R.; Maire J. Insertion Compounds of Graphite with Improved Performances and Electrochemical Applications of those Compounds. U.S. Patent 4584252, April 22, 1986.
29. Mkhoyan, K.; Contryman, A.; Silcox, J.; Stewart, D.; Eda, G.; Mattevi, C.; Miller, S.; Chhowalla, M. Atomic and Electronic Structure of Graphene-Oxide. *Nano Lett.* **2009**, *9*, 1058–1063.
30. Kosynkin, D.; Higginbotham, A.; Sinitskii, A.; Lomeda, J.; Dimiev, A.; Price, K.; Tour, J. Longitudinal Unzipping of Carbon Nanotubes To Form Graphene Nanoribbons. *Nature* **2009**, *458*, 872–876.
31. Eda, G.; Fanchini, G.; Chhowalla, M. Large-Area Ultrathin Films of Reduced Graphene Oxide as a Transparent and Flexible Electronic Material. *Nat. Nanotechnol.* **2008**, *3*, 270–274.
32. Gomez-Navarro, C.; Meyers, J. C.; Sundaram, R. S.; Chuvilin, A.; Kurash, S.; Burghard, M.; Kern, K.; Kaizer, U. Atomic Structure of Reduced Graphene Oxide. *Nano Lett.* **2010**, *10*, 1144–1148.
33. Higginbotham, A.; Kosynkin, D.; Sinitskii, A.; Sun, Z.; Tour, J. M. Lower-Defect Graphene Oxide Nanoribbons from Multiwalled Carbon Nanotubes. *ACS Nano* **2010**, *4*, 2059–2069.
34. Shen, J.; Hu, Y.; Shi, M.; Lu, X.; Qin, C.; Li, C.; Ye, M. Fast and Facile Preparation of Graphene Oxide and Reduced Graphene Oxide Nanoplatelets. *Chem. Mater.* **2009**, *21*, 3514–3520.
35. Gao, W.; Alemany, L.; Ci, L.; Ajayan, P. New Insights into the Structure and Reduction of Graphite Oxide. *Nat. Chem.* **2009**, *1*, 403–408.
36. Cai, W.; Piner, R.; Nguyen, S.; Stadermann, S.; Shaibat, Y.; Yang, D.; Velamakanni, S.; Stoller, M.; An, J.; Chen, D.; Ruoff, R. Synthesis and Solid-State NMR Structural Characterization of 13C-Labeled Graphite Oxide. *Science* **2008**, *321*, 1815–1817.
37. Stankovich, S.; Piner, R.; Nguyen, S.; Ruoff, R. Synthesis and Exfoliation of Isocyanate-Treated Graphene Oxide Nanoplatelets. *Carbon* **2004**, *44*, 3342–3347.
38. Aoi, Y.; Ono, K.; Kamijo, E. Preparation of Amorphous CNx Thin Films by Pulsed Laser Deposition Using a Radio Frequency Radical Beam Source. *J. Appl. Phys.* **1999**, *86*, 2318–2322.
39. Jeong, H.; Lee, Y.; Lahaye, R.; Park, M.; An, K.; Kim, I.; Yang, C.; Park, C.; Ruoff, R.; Lee, Y. Evidence of Graphitic AB Stacking Order of Graphite Oxides. *J. Am. Chem. Soc.* **2008**, *130*, 1362–1366.
40. Gao, X.; Jang, J.; Nagase, H. Hydrazine and Thermal Reduction of Graphene Oxide: Reaction Mechanisms, Product Structures, and Reaction Design. *J. Phys. Chem. C* **2010**, *114*, 832–842.
41. Gilje, S.; Han, S.; Wang, M.; Wang, K. L.; Kaner, R. B. A Chemical Route to Graphene for Device Applications. *Nano Lett.* **2007**, *7*, 3394–3398.
42. Gómez-Navarro, C.; Weitz, R. T.; Bittner, A. M.; Scolari, M.; Mews, A.; Burghard, M.; Kern, K. Electronic Transport Properties of Individual Chemically Reduced Graphene Oxide Sheets. *Nano Lett.* **2007**, *7*, 3499–3503.
43. Sinitskii, A.; Fursina, A. A.; Kosynkin, D. V.; Higginbotham, A. L.; Natelson, D.; Tour, J. M. Electronic Transport in Monolayer Graphene Nanoribbons Produced by Chemical Unzipping of Carbon Nanotubes. *Appl. Phys. Lett.* **2009**, *95*, 253108.
44. Jung, I.; Dikin, D. A.; Piner, R. D.; Ruoff, R. S. Tunable Electrical Conductivity of Individual Graphene Oxide Sheets Reduced at Low Temperatures. *Nano Lett.* **2008**, *8*, 4283–4287.
45. Sinitskii, A.; Dimiev, A.; Kosynkin, D. V.; Tour, J. M. Graphene Nanoribbon Devices Produced by Oxidative Unzipping of Carbon Nanotubes. *ACS Nano* in revision.
46. Sinitskii, A.; Dimiev, A.; Corley, D. A.; Fursina, A. A.; Kosynkin, D. V.; Tour, J. M. Kinetics of Diazonium Functionalization of Chemically Converted Graphene Nanoribbons. *ACS Nano* **2010**, *4*, 1949–1954.
47. Schedin, F.; Geim, A. K.; Morozov, S. V.; Hill, E. W.; Blake, P.; Katsnelson, M. I.; Novoselov, K. S. Detection of Individual Gas Molecules Adsorbed on Graphene. *Nat. Mater.* **2007**, *6*, 652–655.